Article

Analysis and Simulation on a Sequential Rotationally Excited Circularly Polarized Multi-Dipole Antennas Array for Separated GPR in Active Remote Sensing of Deep Earth

Haifeng Fan [1,2], Yiming Zhang [1], Qianqian Tian [3]* and Xuhong Wang [1]

[1] Faculty of Information Technology, Beijing University of Technology, Beijing 100124, China;
[2] Tianjin University of Science and Technology, Tianjin 300457, China;
[3] School of Transportation Science and Engineering, Civil Aviation University of China, Tianjin 300300, China;
hffan@emails.bjut.edu.cn (H.F.); ymzhang@bjut.edu.cn (Y.Z.);wangxuhong@bjut.edu.cn (X.W.).
* Correspondence: qqtian@cauc.edu.cn

Abstract: As an effective active remote sensing (ARS) technology for shallow underground targets, ground penetrating radar (GPR) is a detection method to obtain the characteristic information of underground targets by transmitting electromagnetic wave from the antenna and analyzing the propagation law of the electromagnetic wave underground. Due to the high frequency(1MHz-3GHz) of GPR, the depth of geological exploration is shallow(0.1m-30m). In order to remote sensing the deep earth, it is necessary to increase the size of the radiation source in order to reduce the radiation frequency. At the same time, for most separated GPRs, a single dipole antenna (SD) is used as the radiation source and another antenna device placed along the electromagnetic wave propagation direction in the far field as a remote sensing sensor (RSS), both of which are horizontally linearly polarized (LP) antennas. In some cases, such a design is apt to cause problems such as multipath effect (ME) and polarization mismatch (PM). When GPR in ARS of deep earth is performed, it often results in increased errors, signal attenuation during data reception and processing. In contrast, at the radiation source, with the use of large aperture multiple-dipole antennas (MD) and multi-channel sequential rotational excitation, the electromagnetic wave can radiate outward in the form of circular polarization at a low frequency. At the RSS, the trouble caused by ME and PM can be reduced even if the LP antennas are used. A novel sequential rotationally excited (SRE) circularly polarized (CP) MD array for separated GPR in ARS of deep earth is proposed in this paper, which uses a large aperture CP MD array instead of a small size LP SD. The analysis and simulation results demonstrate that under the premise of the same transmitting power, comparing circular polarization and linear polarization, by using SRE CP MD antennas array radiation source, a significant enhancement (about 7dB) of the Signal to Noise Ratio (SNR) will occur by collecting the radiant energy at the RSS. More importantly, by reducing the exploration frequency to 10KHz, the exploration depth will also be greatly increased by about 10 times.

Keywords: Active remote sensing**;** Sequential rotationally excited; Circularly Polarized; GPR; SNR

1. Introduction

Ground penetrating radar (GPR) technology is an active remote sensing(ARS) method that uses high-frequency(1MHz-3GHz) electromagnetic waves to detect the internal structure of media. After long-term development, it has been applied in many aspects, such as traffic construction and maintenance, water conservancy project detection, urban construction, disaster geological monitoring, environmental research, agricultural geological research and geological structure detection [1-5]. GPR uses a high-frequency electromagnetic wave as the remote sensing carrier, which brings high resolution [6-8], but it also has

 doi:10.20944/preprints202212.0261.v1

the problem of serious attenuation of effective signals. For this reason, the maximum detection depth can only reach about 30m, which severely limits the development of GPR.

As an important part of separated GPR system, transmitting and receiving antennas play a key role in sounding [9-11], resolution and other performance. In 2015, some scholars[12] combined MIMO(multiple-input multiple-output) antenna technology with multi-polarization technology to overcome the interference caused by changes in antenna radiation direction and target scattering cross-sectional area in the measurement process, and significantly improved the detection accuracy of underground targets; The large depth GPR system proposed by Xu Xianlei[13] in 2018 works at 12.5MHz-50MHz, and the corresponding antenna length is 8.25m-2.25m. The corresponding main frequency antenna is used according to the requirements of different detection depths, and the maximum detection depth can reach 80m in coal mine detection with weak attenuation and the positioning accuracy reaches 3 m; In 2019, the lunar exploration radar of the Chinese Academy of Sciences successfully loaded the Chang'e-4 lunar lander with dual-channel antennas (60 MHz and 500 MHz) [14] to obtain a large amount of precious lunar geological data. Different channels correspond to different detection depths and resolutions. However, for large depth GPR remote sensing, conventional methods are difficult to meet.

For most separated GPRs, a single dipole antenna (SD) is used as the radiation source and another antenna device placed along the electromagnetic wave propagation direction in the far field(Ff) as a remote sensing sensor(RSS), both of which are horizontally linearly polarized (LP) antennas. In some cases, such a design is apt to cause problems such as multipath effect (ME) and polarization mismatch (PM) [15]. When GPR in ARS of deep earth is performed, it often results in increased errors, signal attenuation during data reception and processing [16]. ARS refers to a remote sensing system in which a certain form of electromagnetic wave is emitted to the target from the artificial radiation source on the remote sensing platform, and then the reflected wave is received and recorded by the RSS. Its main advantage is that it can operate day and night without relying on solar radiation [17-19], and it can actively choose the wavelength and emission mode of electromagnetic waves according to the purpose of detection. The electromagnetic wave used in ARS is microwave band and laser, and pulse signal is often used. Common radar, side-looking radar, synthetic aperture radar, infrared radar, laser radar and so on are active remote sensing systems [20].

In traditional separated GPR, the electromagnetic wave radiated by the SD is mainly divided into underground direct wave, underground refraction wave, sky wave and side wave [21-23]. As it is horizontal polarization, the electric field propagates parallel to the ground, which will cause large induced current on the ground, resulting in great attenuation of electromagnetic wave. Therefore, the attenuation factor A_h of horizontal polarization wave on the ground and underground is far greater than that of vertical polarization wave(A_v)[24-25]. When the RSS is in the Ff, the direct underground wave and refracted wave attenuate seriously, so the received energy mainly depends on the side wave propagation. Then, along the direction of electromagnetic wave propagation, the corresponding electric field, magnetic field components and phase delay are recorded on the RSS. Further, the Cagniard resistivity is calculated by equation (1). For the reason of LP, when the side wave reaches the RSS, the electric field signal in y-axis is significantly higher than the magnetic field signal in x-axis, which more or less affects the calculation of Cagniard resistivity. Results show that the greater the Signal to Noise Ratio (SNR), the more accurate the Cagniard resistivity calculation [4] is.

$$\rho = \frac{1}{\omega\mu}\left|\frac{E_y}{H_x}\right|^2 \tag{1}$$

where μ is the permeability, and the angular frequency $\omega = 2\pi f$.

When the electromagnetic wave propagates in the form of side waves, it may reach the target directly, or it may reach the ground first, and then reach the target after being reflected by the ground [26]. In addition, it may encounter obstacles such as faults, cavities

Preprints (www.preprints.org) | NOT PEER-REVIEWED | Posted: 15 December 2022 doi:10.20944/preprints202212.0261.v1

and mineral deposits. After being reflected by obstacles, the transmitted wave may also return to the RSS from two paths, namely, directly or after being reflected by the ground or others. Therefore, among the echo signals received by the RSS, in addition to the direct signal directly reflected back to the RSS by the target, there are also the reflected signal reflected back from the ground or others, as well as the signal partially scattered by the ground or others. Because the direct signal and the reflected signal can be regarded as being sent from the same transmitting source, and the two signals are highly correlated or even coherent, it is difficult for conventional antennas to distinguish the real echo signal of the target [27-30]. That is, the wave front is dispersed, so that the electromagnetic wave reaches the RSS along multiple paths. The delayed arrival of the scattering part of the signal will lead to problems such as attenuation, steep wall effect and indirect reception of gloves, causing changes in the amplitude and phase of the echo signal, which will lead to ME [31].

At the same time, for linearly polarization, the maximum induced signal can be obtained only when the polarization direction of the RSS is completely consistent with the polarization direction of the transmitting antenna, otherwise, it will face the loss of polarization isolation above 10dB. During a long-distance transmission of horizontally LP electromagnetic waves, the polarization is easily deflected when encountering obstacles. In this way, the electromagnetic waves will easily cause PM and partial energy loss after reaching the RSS. The LP mode requires a higher directivity of the transmitting antenna, while the radiative electric field vector of circularly polarized (CP) wave rotates along the propagation direction (left or right), and the instantaneous trajectory is circular. When the CP wave encounters an obstacle, the rotation direction will reverse, which can effectively reduce the influence of ME interference. Moreover, the rotating electric field vector has better penetration ability, which can significantly reduce the propagation loss. Therefore, it is widely used in GPS, Beidou, RFID and other communication systems [32-33]. In addition, theoretically, under the same conditions as LP waves, CP waves are divided into horizontal and vertical components at the same time. When LP antennas are used at the RSS, the field intensity of CP waves is 3dB lower than that of LP waves, that is, CP waves can be received by any LP antenna. Although some energy is lost, the RSS does not need to be aligned with the direction of the signal. It can also make up for the ME and PM.

As a conventional radiation source of GPR, the SD is composed of two conductors fed in the center, with a total length of about half a wavelength. After forming an array antenna with multiple SDs, by controlling the amplitude ratio, phase of the current on the SD and spatial position, multiple dipole antennas (MD) can be applied to the base station antenna, CP antenna, MIMO antenna, Yagi antenna and other application scenarios [34]. In this paper, a novel SRE CP MD array for separated GPR in ARS of deep earth is proposed in this paper, which uses a large aperture CP MD array instead of a small size LP SD. The analysis and simulation results demonstrate that under the premise of the same transmitting power, comparing circular polarization and linear polarization, by using SRE CP MD antennas array radiation source, a significant enhancement (about 7dB) of the SNR will occur by collecting the radiant energy at the RSS. More importantly, by reducing the exploration frequency to 10KHz, the exploration depth will also be greatly increased by about 10 times.

2. Principle of SRE circularly polarization

2.1. Interference and superposition principle of electromagnetic wave

Through calculation and simulation, it can be concluded that by placing multiple such SDs perpendicular to each other and building the MD array, the radiation pattern of the E and H-planes of the MD array is symmetrical. If multiple SDs are fed with the same amplitude and 90° phase difference, it is a CP antenna [35].

The electromagnetic waves radiated by each SD constituting the MD array will interfere with and superimpose each other in space [36]. According to this phenomenon, by changing the amplitude and phase excitation of each element of the array, the strength

Preprints (www.preprints.org) | NOT PEER-REVIEWED | Posted: 15 December 2022 doi:10.20944/preprints202212.0261.v1

and weakness of the electromagnetic field in a certain area within the radiation range can be flexibly controlled [37]. Therefore, compared with a single antenna element, the array antenna has a higher degree of freedom in design.

The radiation of the antenna in space is generated by the source current on the antenna. If there are multiple currents meeting the coherence relationship in space, the electromagnetic fields radiated by multiple currents will overlap in space, forming interference [38]. The superposition of electromagnetic waves in the same phase will increase the field strength, while the superposition of electromagnetic waves in the opposite phase will reduce the field strength, which also leads to the uneven distribution of electromagnetic field strength in space. The radiated electromagnetic field generated by current distribution J in a uniform medium can be expressed as:

$$E = -j\omega A - j\frac{1}{\omega\mu\varepsilon}\nabla(\nabla \bullet A) \tag{2}$$

$$H = \frac{1}{\mu}\nabla \times A \tag{3}$$

where A represents the vector magnetic potential. μ represents the relative permeability of the medium and ε represents the relative permittivity of the medium.

According to Helmholtz equation:

$$\nabla^2 A + k^2 A = -\mu J \tag{4}$$

where J represent the current density for linear radiation sources with a linear current density of J , which is also applicable to the surface radiation sources. As shown in figure 1, the linear current density J is along the y-axis direction.

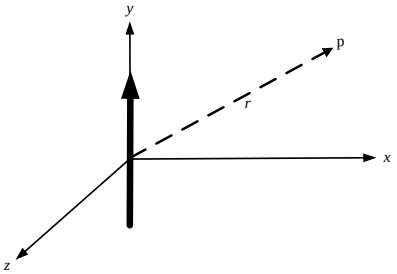

Figure 1. Linear radiation source.

If the line length is L and r represents the distance between the current source and the space observation point, then the superposed magnetic vector A of the field at the space observation point is:

$$A = y\frac{\mu}{4\pi}\int \frac{J_y(y')e^{-jkr}}{r}dy' \tag{5}$$

The integral operation is actually the result of summation of infinitely many parts. If the linear radiation source is equivalent to N small current segments, then the superposition of the magnetic vector of the radiation points in space generated by each segment is the vector magnetic potential of the total radiation field.

$$A_T = \sum_{n=1}^{N} A_n = y\frac{\mu}{4\pi}\sum_{n=1}^{N}\frac{I_n e^{-jkr_n}}{r_n} \tag{6}$$

Therefore, the magnetic vector potential of the total radiation field synthesized somewhere in the space of the linear radiation source with N can be represented by the superposition vector of N magnetic vector potential. Similarly, the surface current source can also be obtained by superposition of N equivalent small current surface radiation fields. Therefore, the discrete current source can be used to replace the continuous current radiator to achieve equivalent electromagnetic wave radiation.

2.2. Principle of pattern multiplication

Preprints (www.preprints.org) | NOT PEER-REVIEWED | Posted: 15 December 2022 doi:10.20944/preprints202212.0261.v1

According to the superposition theory of space electromagnetic waves, the equivalent linear radiation source can be obtained when the tiny antennas are arranged in a linear form. When the tiny antennas are arranged in planar form, the equivalent planar radiation source is obtained. Therefore, for the same antenna element, different array arrangement will obtain different array performance, indicating that array arrangement has a certain impact on the performance of array antenna.

As shown in figure 2, taking the linear array as an example, suppose that the antenna units are arranged at a certain spacing along the x-axis, and assume that the position of each antenna unit is the coordinate x_n from the origin. And the pattern function of each antenna is $F_e(\theta,\varphi)$,which is called unit factor.

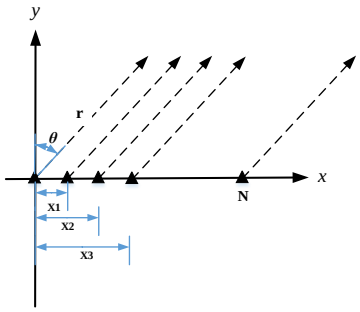

Figure 2. *N*-element linear array.

Assuming that the excitation of each antenna unit is I , the field strength generated by it is positively correlated with the excitation of each antenna unit. Then in spherical coordinates, a point $P(r,\theta,\varphi)$, Then the electric field radiation generated by the Nth antenna unit at point $P(r,\theta,\varphi)$ is:

$$E_N = AI_N \frac{e^{-jkr_N}}{4\pi r_N} F_e(\theta,\varphi) \tag{7}$$

Where, $r_N \approx r - x_N \cos\theta$, taking r_N into the equation (7), according to the principle of spatial electromagnetic wave superposition, the size of the composite electromagnetic field of each unit in the linear array at point $P(r,\theta,\varphi)$ in space is:

$$E_T = \sum_1^N E_N = A\frac{e^{-jkr}}{4\pi r} F_e(\theta,\varphi)\sum_1^N I_N e^{jkx_N\cos\theta} \tag{8}$$

Wherein, $e^{jkx_N\cos\theta}$ represents the relative phase of the electromagnetic wave radiated by each unit to the point $P(r,\theta,\varphi)$ due to the difference of position. Then the array factor is $\sum_1^N I_N e^{jkx_N\cos\theta}$.

From this, it can be seen that the pattern characteristic of the array antenna is equal to the characteristic factor of the element antenna multiplied by the characteristic factor corresponding to the array characteristic.

2.3. Principle of sequential rotationally excited circularly polarization

In practical circular polarization array design, the sequential rotation technique is usually used to achieve symmetrical pattern and improve the axial ratio bandwidth of circular polarization, so as to be used in some broadband applications [35]. The linear polarization unit can be used to achieve good circular polarization performance, and its axial ratio bandwidth is relatively wide. In this method, the antenna elements are rotated 90° successively to arrange their structure. According to the equal feeding amplitude between each element, the feed phase with a sequence difference of 90° is fed to them, so that good circular polarization characteristics can be obtained.

The sequential rotation array technology applied in this paper is to rotate the array position of four antenna elements of any polarization mode by 90° in turn, and it is required that the feeding amplitude between the four elements is equal, and the phase

Preprints (www.preprints.org) | NOT PEER-REVIEWED | Posted: 15 December 2022 doi:10.20944/preprints202212.0261.v1

difference is 90 ° in turn. Using this unique technology, the array antenna composed of linear polarization elements can generate CP electromagnetic waves, while greatly reducing the complexity, weight and feed network loss of the array antenna. Compared with the traditional array arrangement, the mutual coupling between elements can be greatly reduced by using the sequential rotation arrangement, because adjacent elements are placed vertically. In addition, in a wide frequency band, this unique arrangement can enable the main beam to maintain good circular polarization characteristics in a certain angle range away from the maximum radiation direction.

The technology requires that the nth element in an equidistant annular array has a physical rotation angle around the geometric center of the element φ_{pn}, with feed phase shift φ_{en}, the physical rotation angle and feeding phase shall meet the following conditions:

$$\varphi_{pn} = (n-1)\frac{p\pi}{N}, 1 \le n \le N \tag{9}$$

$$\varphi_{en} = (n-1)\frac{p\pi}{N} \tag{10}$$

Where, p is the sequential rotation coefficient and N is the total number of radiation units. For the case of $N=2$ and $p=1$,it can be deduced from the above formula $\varphi_{e1} = \varphi_{p1} = 0$ 、 $\varphi_{e2} = \varphi_{p2} = 90^\circ$ 。 When $N=4$ and $p=2$, the rotation angle and feed phase of each unit are 0°, 90°, 180° and 270°respectively. This configuration is the structure adopted by the sequential rotation array designed in this section.

3. Simulation of SD

Assume that a SD with an arm length of 0.75km is placed along the y-axis in the air domain, and the structure is shown in figure 3. The air domain is a uniform sphere with a radius of 7.5km. Ac excitation of 1000V and 10KHz is performed on the SD lumped port.

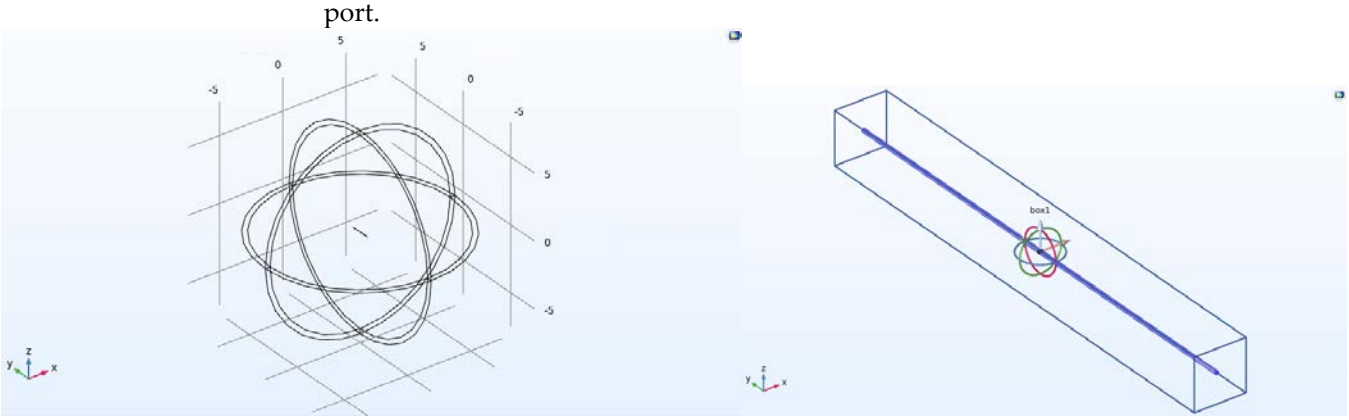

Figure 3. Structure of SD.

Figure 4 shows the distribution and direction of the electric field on the SD plane. It can be seen that the electromagnetic wave propagates outward in the form of linear polarization, and the polarization direction is parallel to the placement direction of the SD.

Preprints (www.preprints.org) | NOT PEER-REVIEWED | Posted: 15 December 2022 doi:10.20944/preprints202212.0261.v1

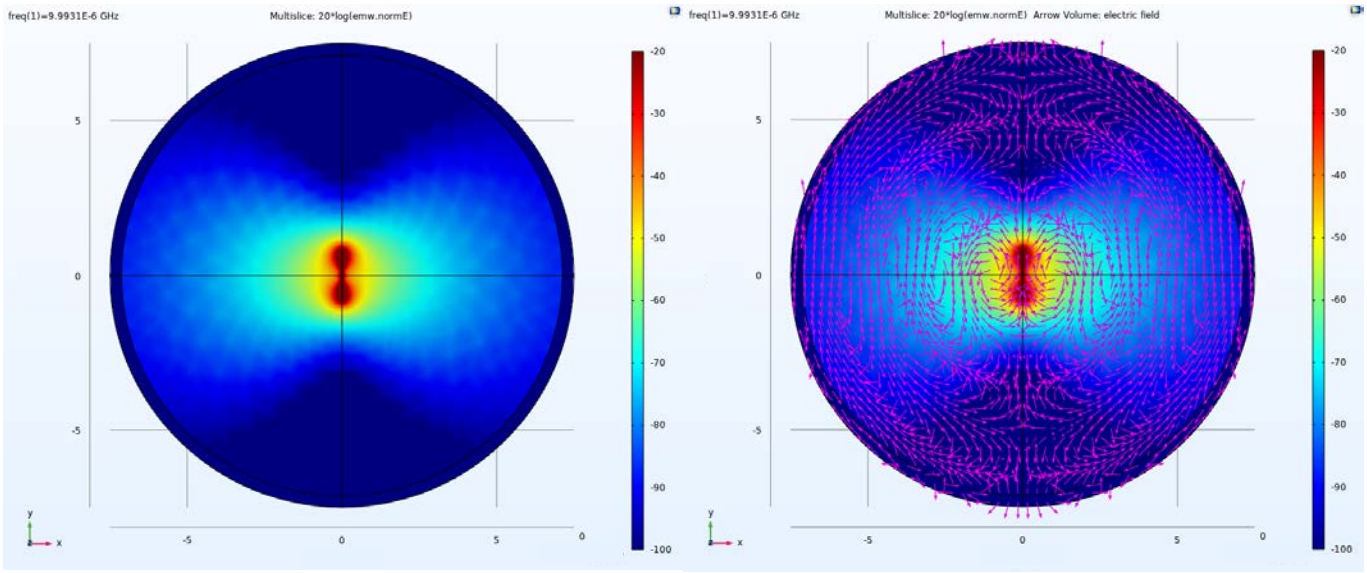

(a) (b)

Figure 4. (a)Electric field distribution and (b)direction of SD.

4. Simulation of SRE circularly polarization based on the MD array

Figure 5 shows the structure of CP MD antennas array model in COMSOL. Four SDs with arm length of 0.75km are placed on four sides of a square area with side length of 1.8km. The feed phase and rotation angle of the four SDs of the array are 0°, 90°, 180° and 270° respectively, and each SD needs to be excited with equal amplitude(1000V) at 10KHz.

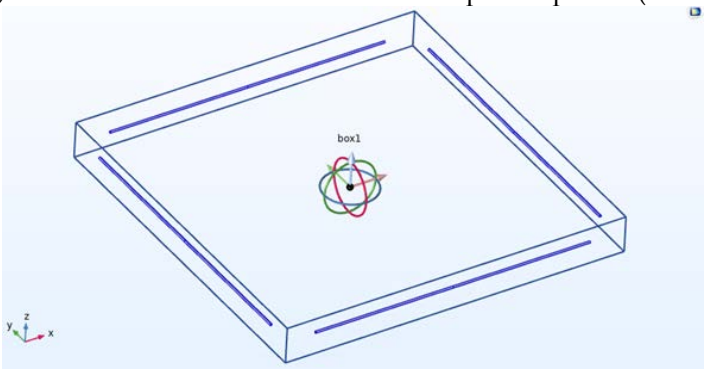

Figure 5. Structure of CP MD antennas array.

4.1. Electric field Simulation of SRE circularly polarization

According to the settings in figure 5, the MD array is placed in the airspace, which is a sphere with a radius of 7.5km. Figure 6 shows the electric field distribution on the MD plane.

Preprints (www.preprints.org) | NOT PEER-REVIEWED | Posted: 15 December 2022 doi:10.20944/preprints202212.0261.v1

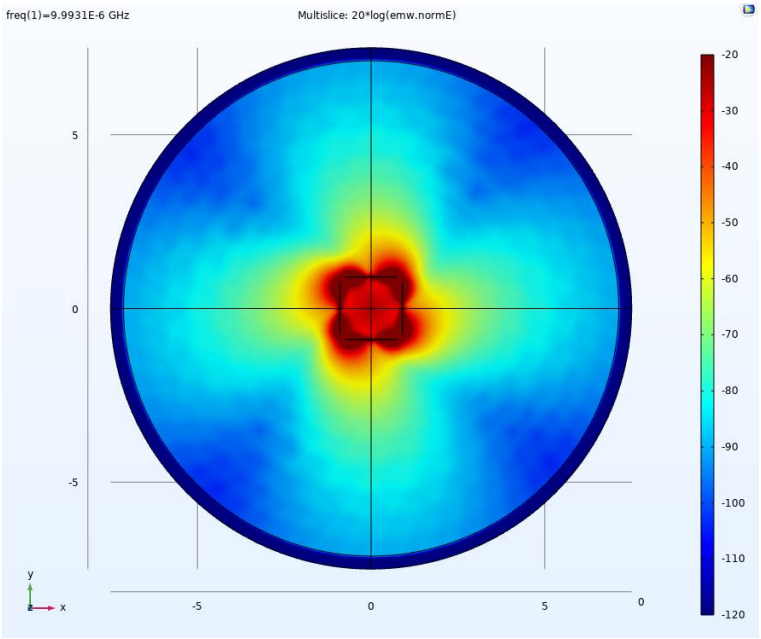

Figure 6. Electric field distribution on MD plane.

It can be seen from figure 6 that the electric field distribution is rearranged and the electric field is rotated after the sequential rotation of the four SDs, completing the transformation from LP to CP.

Figure 7-9 shows the electric field distribution and electric field direction at the height of 0 km, 10 km and 20 km from the MD plane respectively.

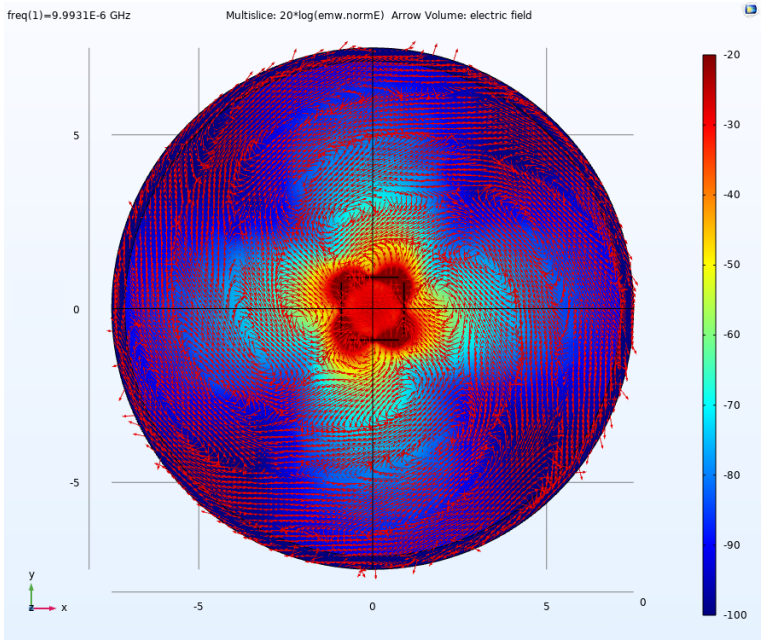

Figure 7. Electric field distribution and direction on MD plane.

Preprints (www.preprints.org) | NOT PEER-REVIEWED | Posted: 15 December 2022 doi:10.20944/preprints202212.0261.v1

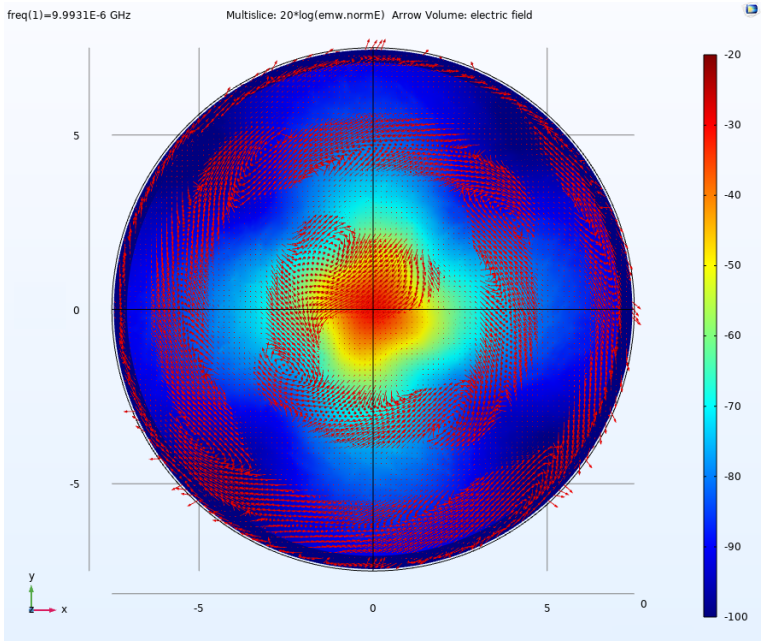

Figure 8. Electric field distribution and direction on the plane 10km above the MD plane.

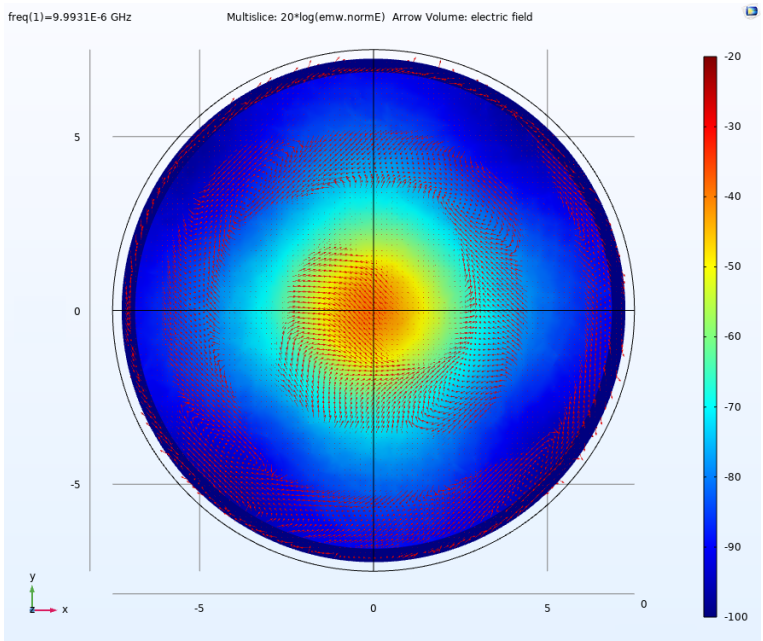

Figure 9. Electric field distribution and direction on the plane 20km above the MD plane.

It can be clearly seen that the electric field rotates in the direction of electromagnetic wave propagation, and the track in the direction of electromagnetic wave propagation is circular, that is, electromagnetic wave propagates in a circular polarized manner.

4.2. Ff Simulation of SRE circularly polarization

From the electric field distribution and electric field direction in the previous section, it can be seen that after the sequential rotation excitation, the linear polarization has completed the conversion to circular polarization. The Ff model can observe the formation process of circular polarization more intuitively. Figure 10(a) shows the two dimensional Ff pattern after circular polarization, while figure 10(b) shows the three dimensional Ff pattern.

Preprints (www.preprints.org) | NOT PEER-REVIEWED | Posted: 15 December 2022 doi:10.20944/preprints202212.0261.v1

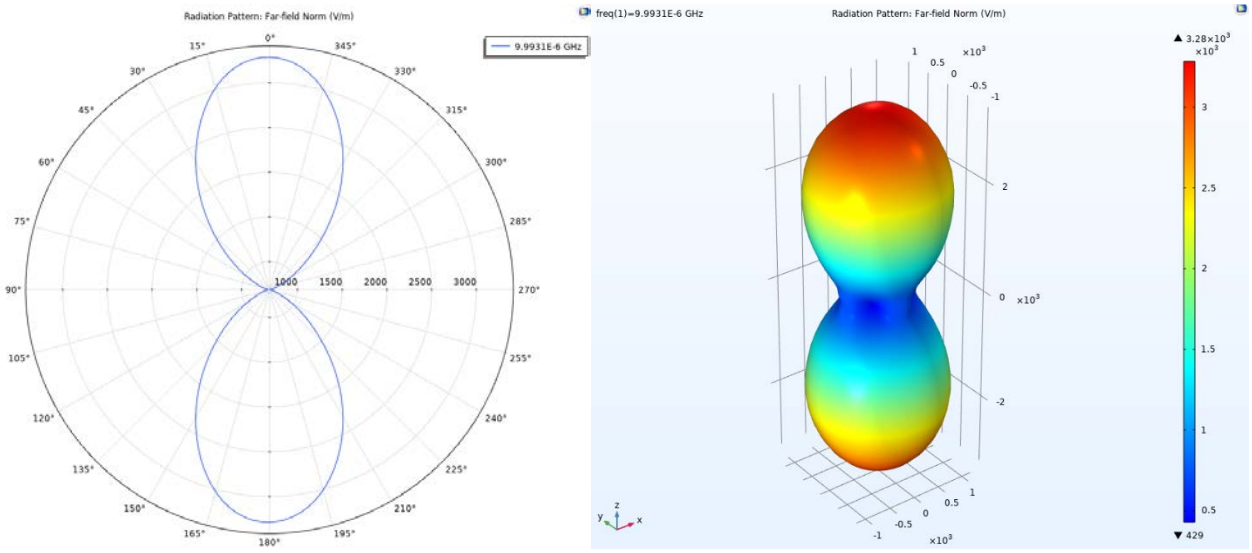

(a) (b)

Figure 10. (a)Two dimensional Ff pattern after circular polarization. (b) Three dimensional Ff pattern after circular polarization.

Figure 10(a) and 10(b) show the circular polarization pattern symmetrical to the MD array plane. It can be seen that the electromagnetic wave propagates in circular polarization mode towards both sides. It can be seen from figure 11 that the shape of the pattern seen from the propagation direction of the electromagnetic wave is circular.

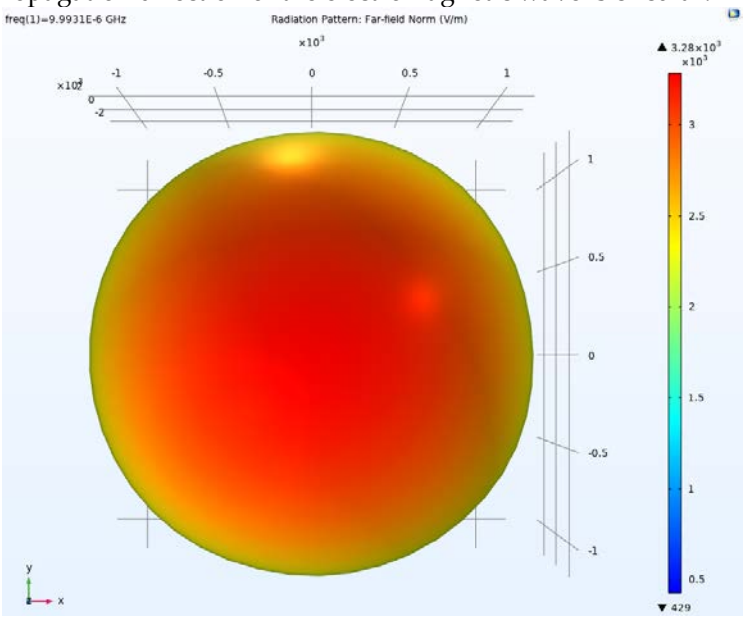

Figure 11. Pattern shape seen along the direction of electromagnetic wave propagation.

5. Simulation of a SRE CP MD antennas array for separated GPR in ARS of deep earth

As illustrated in figure 12, the SRE CP MD antennas array radiation source model is a sphere with a radius of 7.5 km, where the upper half-space is air with $\varepsilon_r = 1$, $\mu_r = 1$and $\sigma = 0 Sm^{-1}$; The lower half-space is soil with $\varepsilon_r = 3$, $\mu_r = 1$and $\sigma = 0.01 Sm^{-1}$.

As shows in figure 12, a SRE CP MD antennas array radiation source for separated GPR was placed on the ground. Four SDs with arm length of 0.75km are placed on four sides of a square area with side length of 1.8km. The feed phase and rotation angle of the four SDs of the array are 0°, 90°, 180° and 270° respectively, and each SD needs to be excited with equal amplitude(1000V) at 10KHz.

Preprints (www.preprints.org) | NOT PEER-REVIEWED | Posted: 15 December 2022 doi:10.20944/preprints202212.0261.v1

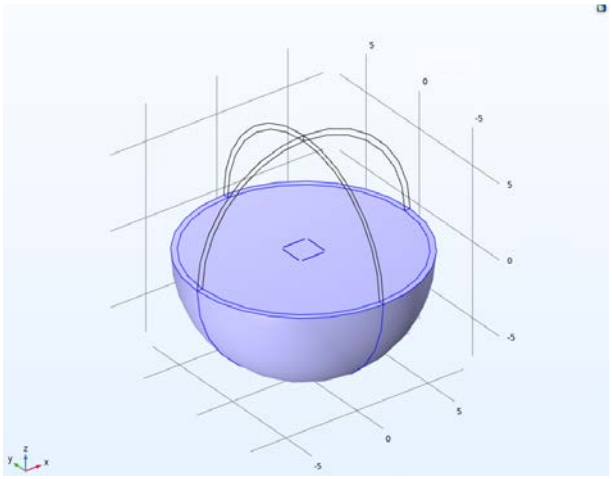

Figure 12. The SRE CP MD antennas array radiation source model.

5.1. Electric field Simulation of a SRE CP MD antennas array for separated GPR in ARS of deep earth

Figure 13-16 shows the electric field distribution and direction on the four sections of the lower half space of the model, that is, the underground space, during the separated GPR in ARS of deep earth. It can be seen that, consistent with the situation in the homogeneous air domain, the electromagnetic wave in the half space model also propagates in the earth in a circular polarization way.

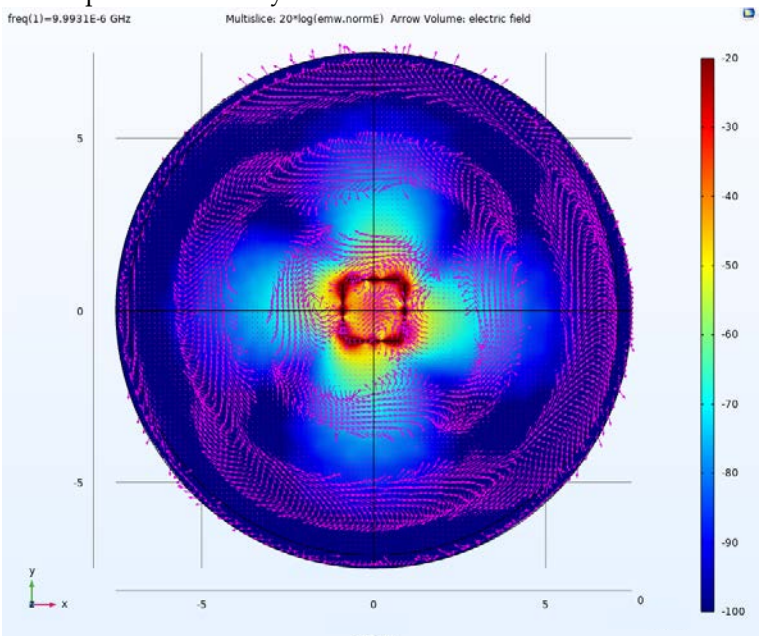

Figure 13. Electric field distribution and direction on the MD plane.

Preprints (www.preprints.org) | NOT PEER-REVIEWED | Posted: 15 December 2022 doi:10.20944/preprints202212.0261.v1

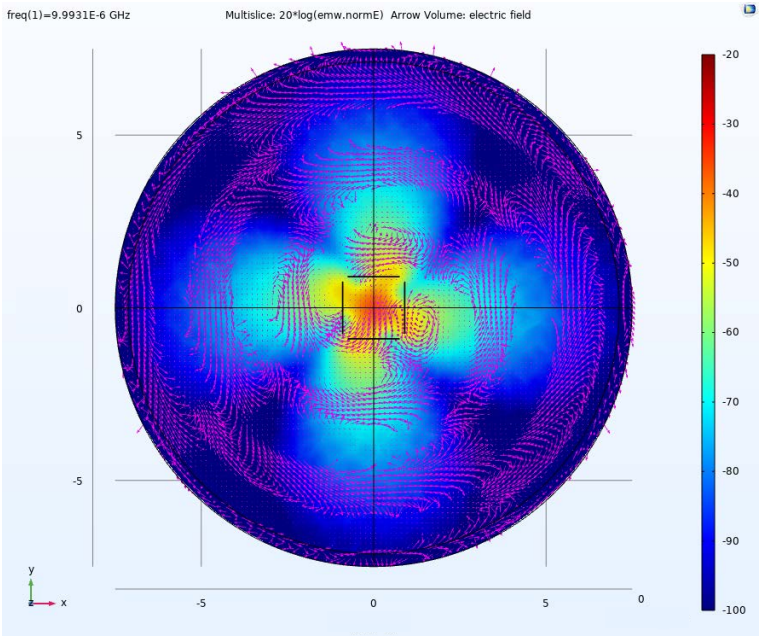

Figure 14. Electric field distribution and direction on the plane 5km below the MD plane.

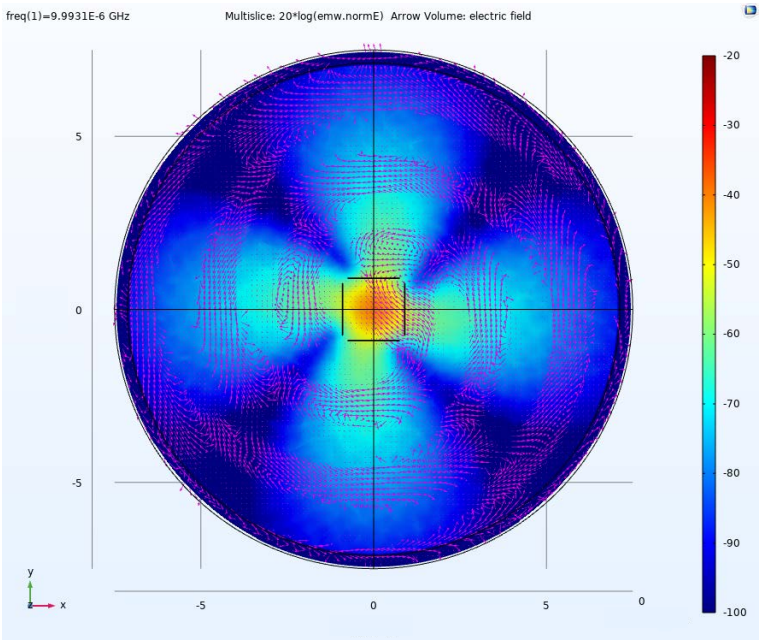

Figure 15. Electric field distribution and direction on the plane 10km below the MD plane.

Preprints (www.preprints.org) | NOT PEER-REVIEWED | Posted: 15 December 2022 doi:10.20944/preprints202212.0261.v1

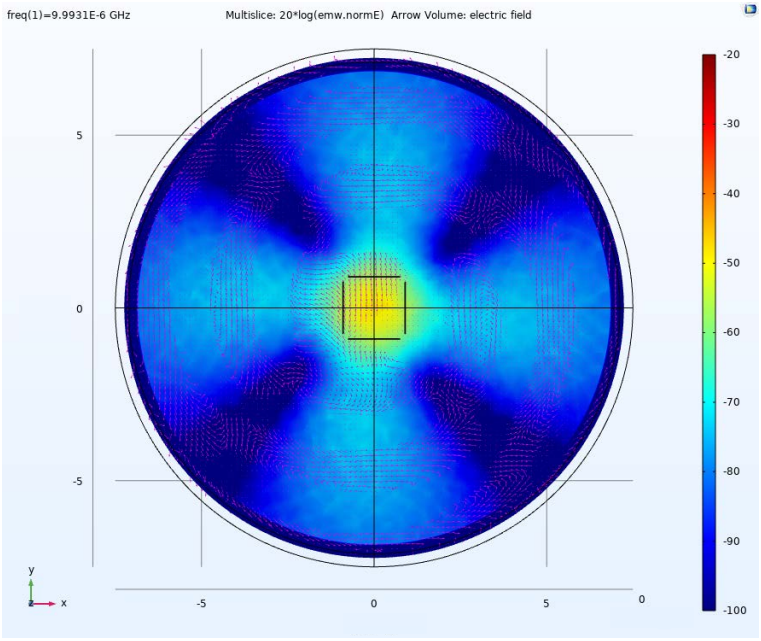

Figure 16. Electric field distribution and direction on the plane 20km below the MD plane.

5.2. Ff Simulation of a SRE CP MD antennas array for separated GPR in ARS of deep earth

The upper half space is the air domain, and the lower half space is the earth. As shown in figure 17, most of the energy propagates towards the air domain, while the electromagnetic waves that penetrate the ground into the air will mostly propagate to the Ff in the form of side waves, which is consistent with the electromagnetic wave propagation mechanism analyzed in the previous chapter.

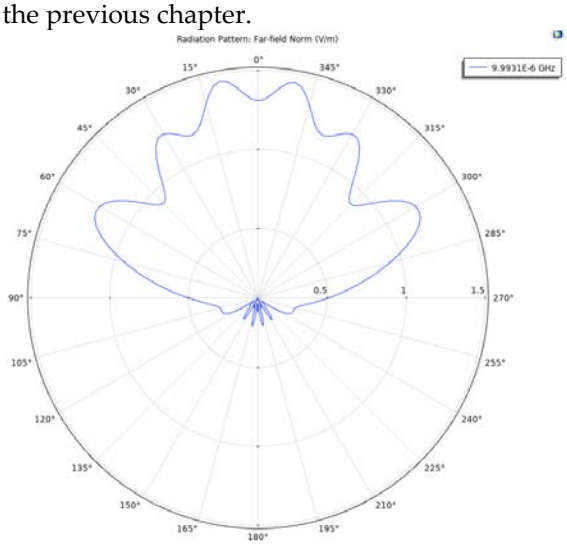

Figure 17. Two dimensional Ff pattern of H-plane.

Figure 18 illustrates that the CP electromagnetic waves emitted by the radiation source are of two types: ground waves and underground waves. The two waves are similar to the waves with inconsistent phases produced by a MD array, because the propagation speed on the ground is much greater than that in the underground. As we all know, the beam propagation direction is always perpendicular to the wave front, at a certain moment, the wave front of both waves will form a synthetic wave front almost parallel to the ground. Consequently, a plane wave with perpendicular incidence will be formed. The plane wave will interact with the underground anomaly and carry information to the RSS on the surface.

Preprints (www.preprints.org) | NOT PEER-REVIEWED | Posted: 15 December 2022 doi:10.20944/preprints202212.0261.v1

Since the RSS is in the Ff, the wave front of electromagnetic wave is almost parallel to the earth after it reaches the RSS position. As shown in figure 18, electromagnetic wave will re-radiate into the earth at a vertical angle. This part of energy will be mainly used for ARS, because electromagnetic wave propagates in the form of circular polarization in this process, while CP electromagnetic wave has stronger penetration and smaller attenuation. Moreover, it can effectively reduce the ME and PM problem, so circular polarization has great advantages over linear polarization.

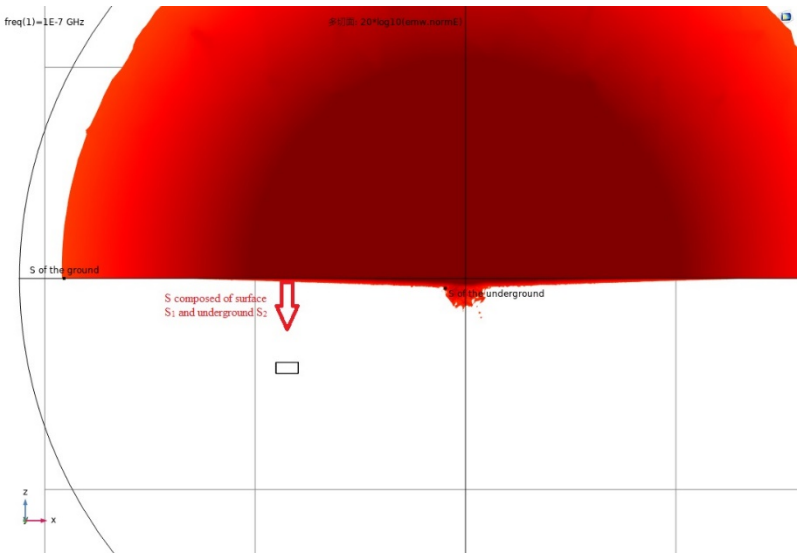

Figure 18. The plane wave principle of the separated GPR in ARS of deep earth, *S* composed of S_1 and S_2, and the direction is vertical downward.

6. Discussion

6.1. Comparison of SNR between LP SD and CP MD for separated GPR in ARS of deep earth

Compared to a traditional LP SD, the SRE CP MD array radiation source will reduce the trouble caused by ME and PM, such as increased errors, signal attenuation during data reception and processing. Moreover, according to equation (1), the stronger the electric field component on the *y*-axis and the magnetic field component on the *x*-axis, the more accurate the calculation of Cagniard resistivity. As the horizontal linear polarization method is used in the conventional method, the component in the *y*-axis is significantly stronger than the component in the *x*-axis, so there is a large error in the calculation of Cagniard resistivity. When the circular polarization method is used for transmission, when the electromagnetic wave reaches the RSS, the electromagnetic field components in *x* and *y* directions are roughly the same order of magnitude, so the calculated resistivity is more accurate.

It is assumed that the power in both cases is 50kW. On the premise of the same total power(TP), through the application of SRE CP MD array, the energy received in the RSS have a higher magnitude than those in the traditional method. Table 1 depicts the excitation of two source modes with the same TP.

Table 1. Excitation of two source modes under the same TP.

Source Mode	Voltage (V)	Current (A)	Phase (deg)	Total Power (kW)
CP MD array	SD_1 250	12.5	0	50
	SD_2 250	12.5	90	
	SD_3 250	12.5	180	
	SD_4 250	12.5	270	
LP SD	1000	50	0	50

Preprints (www.preprints.org) | NOT PEER-REVIEWED | Posted: 15 December 2022 doi:10.20944/preprints202212.0261.v1

Based on Table 2, when the two exploration methods are implemented at different RSS points (the distance ranges from 5km to 10km and the measurement is conducted every 1 km), the energy density time average (Wav) generated by the CP MD array is about five times that of the LP SD during the Ff observation.

Table 2. Comparison of the Wav normalized according to the TP.

Position (*x*, *y*, *z*)	Wav **of** CP MD array	Wav **of** LP SD
(10000, 0, 0)	2.03×10^{-23} J/m³	3.86×10^{-24} J/m³
(9000, 0, 0)	3.59×10^{-23} J/m³	7.22×10^{-24} J/m³
(8000, 0, 0)	5.23×10^{-23} J/m³	1.06×10^{-23} J/m³
(7000, 0, 0)	6.93×10^{-23} J/m³	1.32×10^{-23} J/m³
(6000, 0, 0)	8.55×10^{-23} J/m³	1.69×10^{-23} J/m³
(5000, 0, 0)	1.39×10^{-22} J/m³	2.75×10^{-23} J/m³

According to the SNR calculation formula $S = 10\lg {}^{P_s}\!/_{P_n}$, assuming that the effective Wav received by the RSS is P_{SD} when a LP SD is applied, then the effective Wav received when CP MD is applied is about $5P_{SD}$, and the noise power P_n of both is equal. As can be concluded from table 2, then we can get:

$$S_{SD} = 10\lg\frac{P_{SD}}{P_n}, \tag{11}$$

$$S_{MD} = 10\lg\frac{5P_{SD}}{P_n}. \tag{12}$$

$$S_{MD} - S_{SD} = 10\lg\frac{5P_{SD}}{P_n} - 10\lg\frac{P_{SD}}{P_n} = 10\lg 5 \approx 7dB \tag{13}$$

Where S_{SD} represents the SNR received by the RSS when a LP SD is applied; S_{MD} represents the SNR received by the RSS when a CP MD array is applied.

By subtracting Equation (12) from Equation (11), we can get the Equation (13), the difference between their SNR is about 7dB. In other words, the SNR of CP MD array is better than that of conventional method 7dB, which has obvious advantages in dealing with complex noise environment in the field.

6.2. Comparison of remote sensing depth between the large aperture CP MD array and small size LP SD for separated GPR in ARS

When the separated GPR is used for ARS of deep earth, it can be seen from the previous article that at RSS, electromagnetic waves will vertically shoot into the earth in the form of plane like waves. When the electromagnetic wave propagates in the medium, there is a skin effect, that is, the higher the frequency of the electromagnetic wave, the more obvious the skin effect. It can be seen from the equation (14):

$$\delta = \sqrt{\frac{2\rho}{\omega\mu}} = \sqrt{\frac{2}{\omega\mu\sigma}} = \sqrt{\frac{2}{2\pi f\mu\sigma}} \tag{14}$$

Where δ represents the remote sensing depth; ω represents the angular frequency; μ represents the permeability; ρ represents the resistivity; σ represents the conductivity and f represents the electromagnetic field frequency.

The low frequency of conventional GPR remote sensing frequency is about 1MHz, while the frequency of electromagnetic field can be as low as 10KHz after the application of CP MD array.

$$\frac{\delta_{ARS}}{\delta_{conventional}} = \frac{\sqrt{\frac{1}{f_{ARS}}}}{\sqrt{\frac{1}{f_{conventional}}}} = \sqrt{\frac{f_{conventional}}{f_{ARS}}} = 10 \tag{15}$$

According to equation (15), the remote sensing depth is 10 times deeper than that of conventional methods after the application of the large aperture CP MD array.

 doi:10.20944/preprints202212.0261.v1

7. Conclusions

Herein, a novel SRE CP MD array for separated GPR in ARS of deep earth is proposed in this paper, which uses a large aperture CP MD array instead of a small size LP SD. The analysis and simulation results demonstrate that under the premise of the same transmitting power, comparing circular polarization and linear polarization, by using SRE CP MD antennas array radiation source, a significant enhancement (about 7dB) of the SNR will occur by collecting the radiant energy at the RSS. More importantly, by reducing the exploration frequency to 10KHz, the exploration depth will also be greatly increased by about 10 times.

Firstly, the principle of SRE circularly polarization was presented. Furthermore, the SD, the SRE CP MD antennas array and the SRE CP MD antennas array radiation source for separated GPR in ARS of deep earth are simulated. Then, on the basis of the aforementioned calculations and analysis of SRE CP MD antennas array, several numerical models for the application of SRE CP MD antennas array radiation source with analytical solutions were built. Finally, the effect of SRE CP MD antennas array radiation source was compared with that of conventional methods. The theoretical analysis and simulation results were all consistent, verifying the correctness and effectiveness of the proposed SRE CP MD antennas array radiation source for separated GPR in ARS of deep earth.

Author Contributions: Conceptualization, H.F.; Methodology, H.F.; Visualization, Q.T.; Project administration, Y.Z.; Validation, X.W. All authors have read and agreed to the published version of the manuscript.

Funding: This work was supported by the Beijing Municipal Natural Science Foundation (No. 3214058)

Institutional Review Board Statement: Not Applicable.

Informed Consent Statement: Not Applicable.

Data Availability Statement: Not Applicable.

Acknowledgments: All authors thank the referees, editors and officers of Remote sensing for their valuable suggestions and help.

Conflicts of Interest: The authors declare no conflict of interest.

Abbreviations

ARS	Active remote sensing
GPR	Ground penetrating radar
SD	Single dipole antenna
RSS	Remote sensing sensor
LP	Linearly polarized
CP	Circularly polarized
ME	Multipath effect
PM	Polarization mismatch
MD	Multiple-dipole antennas
SRE	Sequential rotationally excited
SNR	Signal to Noise Ratio
Ff	Far-field
MIMO	Multiple-Input Multiple-Output
TP	Transmitting power
Wav	Energy density time average

References

1. Cui, F.; Bao, J.; Cao, Z.; Li, L.; Zheng, Q. Soil hydraulic parameters estimation using ground penetrating radar data via ensemble smoother with multiple data assimilation. J. Hydrol. 2020, 583, 124552.
2. Léger, E.; Saintenoy, A.; Coquet, Y. Hydrodynamic parameters of a sandy soil determined by ground-penetrating radar inside a single ring infiltrometer. Water Resour. Res. 2014, 50, 5459–5474.

3. Klotzsche, A.; Jonard, F.; Looms, M.C.; van der Kruk, J.; Huisman, J.A. Measuring Soil Water Content with Ground Penetrating Radar: A Decade of Progress. Vadose Zone J. 2018, 17, 180052.
4. Yu, Y.; Weihermüller, L.; Klotzsche, A.; Lärm, L.; Vereecken, H.; Huisman, J.A. Sequential and coupled inversion of horizontal borehole ground penetrating radar data to estimate soil hydraulic properties at the field scale. J. Hydrol. 2021, 596, 126010.
5. Jaumann, S.; Roth, K. Soil hydraulic material properties and layered architecture from time-lapse GPR. Hydrol. Earth Syst. Sci. 2018, 22, 2551–2573.
6. Lambot, S.; Slob, E.C.; Bosch, I.v.d.; Stockbroeckx, B.; Vanclooster, M. Modeling of ground-penetrating Radar for accurate characterization of subsurface electric properties. IEEE Trans. Geosci. Remote Sens. 2004, 42, 2555–2568.
7. Davis, J.L.; Annan, A.P. Ground-penetrating radar for high-resolution mapping of soil and rock stratigraphy1. Geophys. Prospect. 1989, 37, 531–551.
8. Tran, A.P.; Bogaert, P.; Wiaux, F.; Vanclooster, M.; Lambot, S. High-resolution space–time quantification of soil moisture along a hillslope using joint analysis of ground penetrating radar and frequency domain reflectometry data. J. Hydrol. 2015, 523, 252–261.
9. Yu, Y.; Huisman, J.A.; Klotzsche, A.; Vereecken, H.; Weihermüller, L. Coupled full-waveform inversion of horizontal borehole ground penetrating radar data to estimate soil hydraulic parameters: A synthetic study. J. Hydrol. 2022, 610, 127817.
10. Feng, X.; Ren, Q.; Liu, C.; Zhang, X. Joint acoustic full-waveform inversion of crosshole seismic and ground-penetrating radar data in the frequency domain. Geophysics 2017, 82, H41–H56.
11. Serbin, G.; Or, D. Ground-penetrating radar measurement of soil water content dynamics using a suspended horn antenna. IEEE Trans. Geosci. Remote Sens. 2004, 42, 1695–1705.
12. Zeng, Z.F.; Li, J.; Huang, L.; Feng, X.; Liu, F.S. Improving Target Detection Accuracy Based on Multi polarization MIMO GPR. IEEE Transactions on Geoscience and Remote Sensing. 2015, 53,15-24.
13. Xu, X.L. Development of vehicle mounted ground penetrating radar system and experimental research on its application. China University of Mining and Technology (Beijing), 2013.
14. Lai, J.L.; Xu, Y.; Zhang, X.P.; Xiao, L.; Yan, Q.; Meng, X.; Zhou, B.; Dong, Z.H.; Zhao, D. Comparison of Dielectric Properties and Structure of Lunar Regolith at Chang'e-3 and Chang'e-4 Landing Sites Revealed by Ground-Penetrating Radar. Geophysical Research Letters. 2019, 46,12783-12793.
15. Bano, M. Modelling of GPR waves for lossy media obeying a complex power law of frequency for dielectric permittivity. Geophys. Prospect. 2004, 52, 11–26.
16. Brosten, T.R.; Day-Lewis, F.D.; Schultz, G.M.; Curtis, G.P.; Lane, J.W. Inversion of multi-frequency electromagnetic induction data for 3D characterization of hydraulic conductivity. J. Appl. Geophys. 2011, 73, 323–335.
17. Bano, M.; Tsend-Ayush, N.; Schlupp, A.; Munkhuu, U. Ground-Penetrating Radar Imaging of Near-Surface Deformation along the Songino Active Fault in the Vicinity of Ulaanbaatar, Mongolia. Appl. Sci. 2021, 11, 8242.
18. Lavoué, F.; Brossier, R.; Métivier, L.; Garambois, S.; Virieux, J. Two-dimensional permittivity and conductivity imaging by full waveform inversion of multi offset GPR data: A frequency-domain quasi-Newton approach. Geophys. J. Int. 2014, 197, 248–268.
19. Busch, S.; van der Kruk, J.; Bikowski, J.; Vereecken, H. Quantitative conductivity and permittivity estimation using full-waveform inversion of on-ground GPR data. Geophysics 2012, 77, H79–H91.
20. Jin,R.; Lee,K.S. Investigation of Forest Fire Characteristics in North Korea Using Remote Sensing Data and GIS. Remote Sens. 2022, 14, 5836.
21. Shlykov, A.A.; Saraev, A.K. Wave effects in the field of a high frequency horizontal electric dipole. Izvestiya-Physics of the Solid Earth. 2014, 50, 249-14.
22. Unsworth, M.J.; Travis, B.J.; Chave, A.D. Electromagnetic induction by a finite electric dipole source over a 2D earth. Geophysics. 1993, 58,198-17.
23. Hobbs, B.; Ziolkowski, A.; Wright, D. Multi-Transient Electromagnetics (MTEM)-controlled source equipment for subsurface resistivity investigation, in 18th IAGA WG. 2006, 1, 17-23.
24. Kuznetzov, A.N. Distorting effects during electromagnetic sounding of horizontally non-uniform media using an artificial field source. Earth Physics.1982, 18, 130-137.
25. Wang, X.X.; Di, Q.Y.; Xu, C. Characteristics of Multiple Dipole Sources and Tensor Measurement in CSAMT. J. Geophys. 2014, 57, 651–661.
26. Radzevicius, S.J.; Daniels, J.J.; Guy, E.D.; Vendl, M.A. Significance of crossed-dipole antennas for high noise environments. Proc. Symp. Appl. Geophys. Eng. Environ. Probl. 2000, 407–413. https://doi.org/10.3997/2214-4609-pdb.200.2000_048
27. Liu, L.; Wang, C. Two-dimensional DOA estimation based on polarization sensitive array and uniform linear array. J. Electron. Inf.Technol. 2019, 41, 2350–2357.
28. Huang, Y.; Barkat, M. Near-field multiple source localization by passive sensor array. IEEE Trans. Antennas Propag. 1991, 39, 968–975.
29. Ma, H.; Tao, H.; Xie, J. Mixed far-field and near-field source localization using a linear tripole array. IEEE Wirel. Commun. Lett. 2020, 9, 889–892.
30. Ma, H.; Tao, H.; Kang, H. Mixed far-field and near-field source localization using a linear electromagnetic-vector-sensor array-with gain/phase uncertainties. IEEE Access. 2021, 9, 132412–132428.

 doi:10.20944/preprints202212.0261.v1

31. Zhao, L.; Tao, H.; Chen,W.; Song, D. Maneuvering target detection based on subspace subaperture joint coherent integration. Remote Sens. 2021, 13, 1948.
32. He, J.; Ahmad, M.O.; Swamy, M.N.S. Near-field localization of partially polarized sources with a cross-dipole array. IEEE Trans. Aerosp. Electron. Syst. 2013, 49, 857–870.
33. Yuan, X. Coherent sources direction finding and polarization estimation with various compositions of spatially spread polarized antenna arrays. IEEE Signal Process. 2014, 102, 265–281.
34. Zhao, Y.; Zhang, Q.; Tang, B. Frequency diversity array MIMO track-before-detect in coherent repeated interference. IEICE Transactions on Fundamentals of Electronics. Commun. Comput. Sci. 2018, 10, 1703–1707.
35. He, J.; Li, L.; Shu, T. Near-field parameter estimation for polarized source using spatial amplitude ratio. IEEE Commun. Lett. 2020,24, 1961–1965.
36. Sedighi, S.; Rao, B.; Ottersten, B. An asymptotically efficient weighted least squares estimator for co-array-based DOA Estimation.IEEE Trans. Signal Process. 2020, 68, 589–604.
37. Fan, H.F.; Zhang, Y.M.; Wang, X.H. An Asymmetric Beamforming Method Based on Arithmetic Phase Difference Weighting in CSAMT. Symmetry. 2022, 14, 2374.
38. Lehmann, F.; Boerner, D.E.; Holliger, K.; Green, A.G. Multicomponent georadar data: Some important implications for data acquisition and processing. Geophysics 2000, 65, 1542–1552.